Annals of Biomedical Engineering, Vol. 24, pp. 430–439, 1996
Printed in the USA.

0090-6964/96 $10.50 + .00

Multimodality Multidimensional Image Analysis of Cortical and Subcortical Plasticity in the Rat Brain

ALBERTO F. GOLDSZAL,*† OLEH J. TRETIAK,† DEMERAL D. LIU,‡ and PETER J. HAND§

*National Institutes of Health, National Institute on Aging, GRC, LPC, Baltimore, MD; †Imaging and Computer Vision Center, Drexel University, Philadelphia, PA; ‡Mahoney Institute of Neurological Science, University of Pennsylvania, Philadelphia, PA; and §Department of Animal Biology, School of Veterinary Medicine, University of Pennsylvania, Philadelphia, PA

Abstract—In this work, we developed and implemented a multimodality multidimensional imaging system which is capable of generating and displaying anatomical and functional images of selected structures and processes within a vertebrate's central nervous system (CNS). The functional images are generated from [^{14}C]-2-deoxy-D-glucose (2DG) autoradiography whereas the anatomic images are derived from cytochrome oxidase (CO) histochemistry. This multi-modality imaging system has been used to study mechanisms underlying information processing in the rat brain. We have applied this technique to visualize and measure the plasticity (deformation) observed in the rat's whisker system due to neonatal lesioning of selected peripheral sensory organs. Application of this imaging system revealed detailed information about the shape, size, and directionality of selected cortical and subcortical structures. Previous 2-D imaging techniques were unable to deliver such holistic information. Another important issue addressed in this work is related to image registration problems. We developed an image registration technique which employs extrinsic fiduciary marks for alignment and is capable of registering images with subpixel accuracy. It uses the information from all available fiduciary marks to promote alignment of the sections and to avoid propagation of errors across a serial data set.

Keywords—Multimodality imaging, Image registration, Brain mapping, Brain plasticity, Rat brain, Imaging

INTRODUCTION

In diagnostic and research applications, the interpretation of brain images is greatly enhanced when different data sets are compared in the same coordinate system. The ability to integrate information collected by different imaging modalities has great potential for answering basic and clinical problems in the neurosciences. For instance, imaging modalities like positron emission tomography (PET), single photon emission computed tomography (SPECT), and functional magnetic resonance imaging (fMRI) can provide information about brain function, allowing the study of hemodynamics, pharmacokinetics, and metabolism *in vivo*. However, although these functional imaging modalities often exhibit excellent contrast between different tissues, they suffer from low signal-to-noise ratio (SNR) and poor spatial resolution. Therefore, the understanding of brain function is greatly enhanced when functional images are complemented with the underlying anatomy visible on other imaging modalities, such as magnetic resonance imaging (MRI) and computerized tomography (CT).

Some examples involving multimodality imaging of the brain can be found in the work of Apicella *et al.* (1); the combination of CT, MRI, and PET images by Pelizzari *et al.* (19); the use of stereotactic coordinate systems for anatomical-functional correlative studies by Evans *et al.* (8); and the work of Ogawa *et al.* (18), which employs MRI and fMRI. All of the above-mentioned investigators use multimodality imaging systems to obtain better anatomical localization of functional activity in the brain. This information has been used in radiation therapy, surgical planning, cognitive studies, and brain mapping.

Multimodality three-dimensional imaging has become increasingly important in clinical environments, particularly for the diagnosis and treatment of brain disorders like epilepsy, Alzheimer's disease, and multiple sclerosis. Its importance to neuroscience has also been demonstrated (7,9,20). In this paper, we introduce a multimodality imaging system applied to vertebrate brain mapping. This imaging system is capable of handling a massive number of misaligned sliced data and providing relevant anatomical and functional information on macroscopic structures in two- and three-dimensional space.

This multimodality multidimensional imaging system has been used to study the plasticity (deformation) phenomena in the rat's vibrissal representation after neonatal lesion of the sensory organ. The functional (metabolic) images are obtained with the [^{14}C]-2-deoxy-D-glucose (2DG) autoradiographic technique after Sokoloff *et al.*

Acknowledgment—This work was partially supported by NIH grant P41RR01638, NIH grant NS22283, and CAPES (Ministry of Education, Brazil) grant 2410/89-2.

Address correspondence to Dr. Alberto F. Goldszal, National Institutes of Health, National Institute on Aging, Gerontology Research Center, Laboratory of Personality and Cognition, Box 03, 4940 Eastern Avenue, Baltimore, MD 21224, U.S.A.

(Received 5May95, Revised 11Aug95, Revised 21Nov95, Accepted 28Nov95)

(24), whereas the anatomical images are obtained from cytochrome oxidase (CO) histochemistry after Wong-Riley (27). Using these two imaging modalities, we have studied and analyzed several cases of altered functional and anatomical organization in the cortical and subcortical representations of vibrissa columns in developmentally lesioned rats. The application of this imaging technique has demonstrated that it is possible to obtain more insight and understanding of the structures and processes being imaged than when using previously developed techniques.

FUNCTIONAL AND ANATOMICAL IMAGING IN EXPERIMENTAL BIOLOGY

Functional Imaging

In our work, we employ quantitative autoradiography as the functional imaging modality and cytochrome oxidase staining as our anatomical imaging source. Quantitative autoradiography can measure many functional parameters on a regional basis in the brain, including local hemodynamics, metabolism, and pharmacokinetics. The general procedure was best summarized by McEachron *et al.* (17): "[It] involves the injection of a radiolabelled compound followed by a predetermined waiting period during which the compound is distributed throughout the body. In most instances, an environmental or pharmacological stimulus is applied during the waiting period and changes in the pattern of the radiotracer's distribution are correlated with the stimulus. After that time, the animal is sacrificed, the brain removed and frozen to prevent diffusion of the tracer. The brain is then thin sectioned in a cryostat and the sections placed in contact with photographic emulsion, most often X-ray film. The radioactive decay of the isotope causes a latent image to form on the film through an interaction with the silver halide crystals in the emulsion."

A large number of different radiotracers can be employed in functional mapping using the above protocol. One commonly employed tracer is [^{14}C]-2-deoxy-D-glucose—2DG for short—developed by Sokoloff *et al.* (24) for the purpose of studying local cerebral metabolism *in vivo*. This analog tracer of glucose is transported into the brain by the same carrier as glucose and, similarly, is subsequently phosphorylated by hexokinase; however, the product of this reaction—[^{14}C]-deoxyglucose-6-phosphate—is essentially trapped inside the brain for the duration of the study. This radioactive product thus builds up in proportion to the intensity of the applied stimulus, quantitatively marking anatomical sites of functional activity.

The 2DG method can provide information concerning functional organization of large arrays of neurons. For example, it is possible to study the functional connectivity of an entire sensory pathway, such as that of the rat's whisker system, within an individual animal. Such mapping is possible because of the close link between brain metabolism, which in the adult is almost entirely dependent upon glucose, and neural function (11,24). In the case of mapping studies, the increased neural activity produces an increased demand for, and uptake of, glucose as well as [^{14}C]-2DG. Thus, structures of the activated neural system become more densely labeled than those of nonstimulated systems.

Anatomical Imaging

The anatomical images used in our experiments were generated with cytochrome oxidase histochemistry (27). Cytochrome oxidase is an endogenous enzyme found in neurons. Its usage is intimately associated with the neurons' metabolic machinery, which is in turn closely related to the levels of neuronal activity. CO belongs to a group of energy-deriving enzymes. They are responsible for electron transport and oxidative phosphorylation, yielding adenosine triphosphate (ATP). ATP is related to essential processes such as protein synthesis, maintenance of the resting membrane potential, and rapid axoplasmic transport within neurons; therefore, it can be reasoned that more active neurons would be more vigorously involved with the above processes and, as a consequence, would develop more active cytochrome systems (27).

Previous studies (27) have indicated that the detection of cytochrome oxidase enzymes in neurons of the central nervous system (CNS) correlates directly with the morphology of the structures being studied. Therefore, the histological sections that produced the autoradiographic images can be stained to detect cytochrome oxidase enzymes to produce anatomical (or morphological) descriptors of functional processes.

Figure 1 shows a two-dimensional (2-D) multimodality image of a coronal section through a rat's brain, which was submitted to stimulation of a selected structure in the sensory system (Experimental Design). The image on the left was generated with the 2DG autoradiographic technique and represents rates of glucose utilization. The image on the right, produced with CO histochemistry, is the corresponding anatomical representation of the 2DG image.

Imaging anatomical and metabolic (functional) structures and/or processes within the vertebrate's CNS becomes possible through the combination of the abovementioned techniques. However, multidimensional representations of both metabolism and anatomy, particularly autoradiograms and the corresponding histological sections, still remain a big challenge. Some of the problems are associated with tissue degeneration after exposure to radiotracers and during sectioning, resulting in poor staining quality of these tissues and, consequently, low-quality (anatomical) images. On the functional imaging side, the

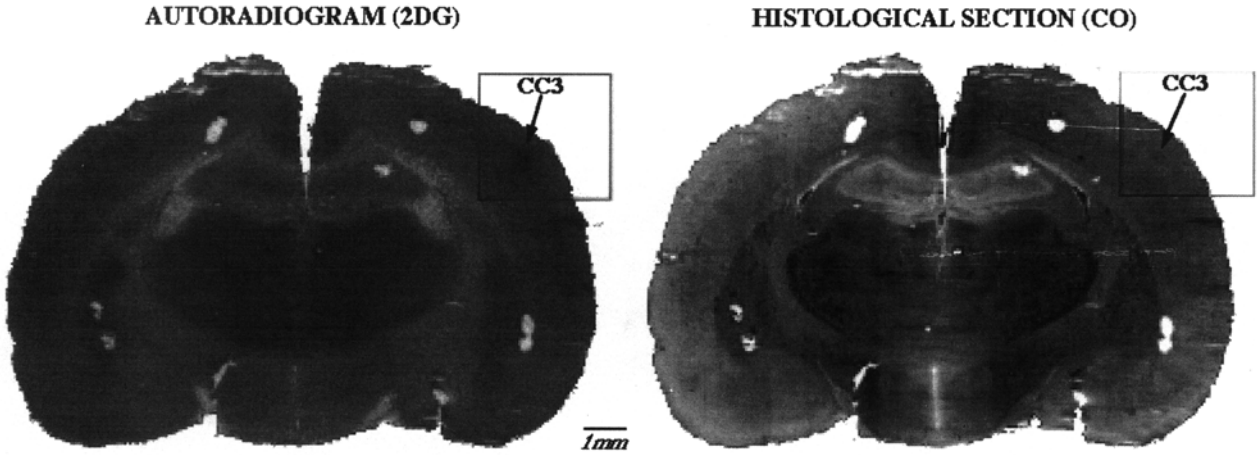

FIGURE 1. Two-dimensional multimodality images of a coronal section through a rat's brain. The animal underwent unilateral stimulation of the C3 whisker, part of the sensory system. The image on the left was generated with the 2DG autoradiographic technique and represents rates of glucose utilization. The image on the right, produced with CO histochemistry, is the corresponding anatomical representation of the 2DG image. Six fiduciary marks, employed for registration of the sections, are visible on these images.

problems are associated with the tracing technique. Since the 2DG method is dependent on glucose metabolism for its effects, and because of the fact that neurons of the CNS have a relatively large basal metabolic rate for glucose, the methodology generates a lower signal-to-noise ratio (SNR) of autoradiographic labeling than do other tracing methods (*e.g.*, axoplasmic flow tracers).

The use of other imaging modalities (*e.g.*, MRI, fMRI, CT, and PET) to image anatomical and functional structures within a vertebrate's CNS has generated a lot of enthusiasm. This is an extremely active field. However, even these imaging techniques have provided limited information because of constraints related to spatial and temporal resolutions, localization of the site of activation, and limited availability of contrast agents.

IMAGE REGISTRATION

Image registration is an essential intermediate step used in any multimodality multidimensional imaging system. Autoradiograms and CO-stained sections are acquired on a per-slice basis; therefore, to reposition the sliced data in a way consistent with their source volumes and to correctly align autoradiograms and histological sections of the same structure, it is essential to perform the registration as accurately as possible.

Image registration algorithms can make use of either extrinsic or intrinsic features for alignment. Extrinsic features (*e.g.*, introduced fiduciary marks) can be formed by using suitable objects external to the brain, or, as in our work, placing registration marks in the brain itself (9). Intrinsic registration is based on features that occur naturally in the images being aligned. Intrinsic methods can be based on moments (15), correlation (10,12), distance functions (4,26), or anatomical landmarks already present in the images. Most of our materials—tangential sections within the first somatosensory (SI) area of the rat neocortex—are poor in the sorts of features required by intrinsic methods, so we used an extrinsic registration procedure.

The developed registration method used in this work, named the Multi-Set Registration (MSR) algorithm, is able to perform subpixel registration of the images being aligned based on the two or more fiduciary marks. A detailed description of the method can be found in Ref. 9. For now, we will present the theoretical framework and the major steps of the MSR algorithm.

The MSR technique is based on the Procrustean analysis (22,23) for minimization of the residual registration error. This technique has produced alignment of serial sections with equal or greater accuracy than previously published techniques, like the singular value decomposition (SVD) of Arun *et al.* (2) and the geometric alignment method of Toga *et al.* (25). The MSR method has also presented better registration accuracy than intrinsic methods, such as the Chamfer technique implemented by Borgerfors (5) and the moments method by Hibbard and Hawkins (13). A comparison of the MSR method with other previously developed techniques will be presented in the next section (Accuracy of Registration).

We start defining the registration model as follows:

$$f(i,j) = R(j)p(i) + t(j) + n(i,j),$$

where $f(i,j)$ are data points, $i = 1 \ldots n$ are the number of fiduciary marks used for alignment, and $j = 1 \ldots m$ are the number of slices to be aligned; $p(i)$ is the true (unknown) location of the fiducial points in the reference coordinate system; $R(j)$ and $t(j)$ are, respectively, the rotation and translation of the jth frame; and $n(i,j)$ are mea-

surement errors. Typically, we assume that the first section is in the reference coordinate frame, so that $R(1) = I$ and $t(1) = 0$.

The residual error after alignment is then defined as

$$\epsilon = \sum_{i,j} \|f(i,j) - R(j)p(i) - t(j)\|^2.$$

This equation is different from the original residual error definition given by the Procrustean analysis. In our formulation, we find the best location for the fiducial points, $p(i)$, as well as the best rotations, $R(j)$, and translations, $t(j)$, of the serial sections that minimize the total residual error. In the original Procrustean analysis (22,23), the alignment is performed on a pairwise basis, and only the computation for the best translations and rotations is included in the minimization procedure. One of the advantages of our formulation is the fact that errors that occurred during alignment of two adjacent slices are not propagated throughout the 3-D data set.

An isotropic scaling correctional factor is also included in our algorithm (14). This is necessary because we have observed that, in general, tissue sections shrink after exposure to histochemical stains; therefore, a correctional scaling transformation must be applied between a histological section and its corresponding autoradiographic image. It is also possible to correct anisotropic scaling between data sets. Elastic matching techniques (3,6) are especially suitable for that task. In this work, however, we have observed that any shrinkage or expansion of the sections can be modeled as isotropic transformations.

ACCURACY OF REGISTRATION

To measure the accuracy of the MSR algorithm, we compared it against four previously developed registration techniques: the singular value decomposition (SVD) of Arun *et al.* (2), the geometric alignment method (GM) of Toga *et al.* (25), the Chamfer technique (CHAMFER) developed by Borgerfors (5), and the moments method (MOMENTS) by Hibbard and Hawkins (13).

For this comparison test, we created a 3-D misaligned data set containing 50 adjacent sections, each having six fiduciary marks. This 3-D test set was formed by scanning one section and then transforming it with random translations (limited to -20 to $+20$ pixels), random rotations (between 0° and 60°), and additive gaussian noise. The histological section (cytochrome oxidase) in Fig. 1 illustrates the seminal section. We employed three of the fiduciary marks (alignment fiducials) for registration of the serial sections, and the remaining three marks (control fiducials)—not employed during alignment—were used to measure the algorithm's registration accuracy through computation of the r.m.s. residual error. (The CHAMFER and MOMENTS techniques do not employ fiduciary marks for alignment; nevertheless, to keep consistency throughout the test, we also reported the accuracy of these registration methods based on the final position of the control fiducials.)

TABLE 1. Comparison among different registration techniques using the same 3-D test set.

Registration technique	Error on control fiducials (mean ± SD)
MSR	0.89 ± 0.26
GM	1.90 ± 0.63
SVD	1.32 ± 0.24
MOMENTS	1.75 ± 0.52
CHAMFER	1.61 ± 0.45

Refer to the text for details. The residual error after registration is reported in pixel dimensions.

We repeated the above protocol using all possible combinations of control and alignment fiduciary marks (groups of three) and report the overall residual error and standard deviations for all trials in Table 1. The same protocol and test set was applied to all five registration methods being compared. We should also mention that for the MSR, SVD, and GM techniques, the centroids of the alignment fiducials were used as input. A centroid is computed by first isolating the fiduciary mark with a double thresholding function and then computing its center of mass through calculation of the first-order moments (15). The same procedure was applied for computation of the centroids of the control fiducials.

Additionally, the CHAMFER and MOMENTS techniques required a preprocessing step. For the CHAMFER method, the images were first binarized with a global thresholding function and the registration performed through minimization of generic distance transform between the outlines of the images. The MOMENTS technique employed the binary images to compute the first- and second-order moments for registration. The former technique has been implemented in the ANALYZE software (21), whereas the later was used with the BRAIN software (26).

The results are listed in Table 1. They indicate that the

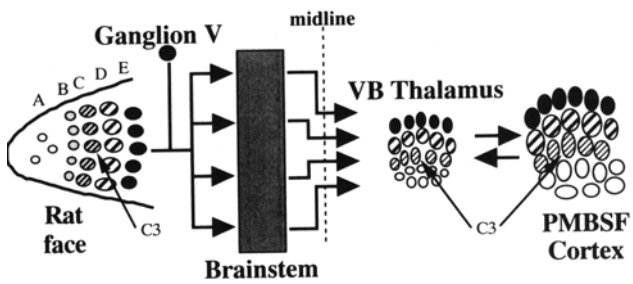

FIGURE 2. Schematic representation of the sensory pathway between vibrissae located at the rat's face and the corresponding barreloids in the VB thalamus and in the PMBSF of SI cortex. Adapted from (28).

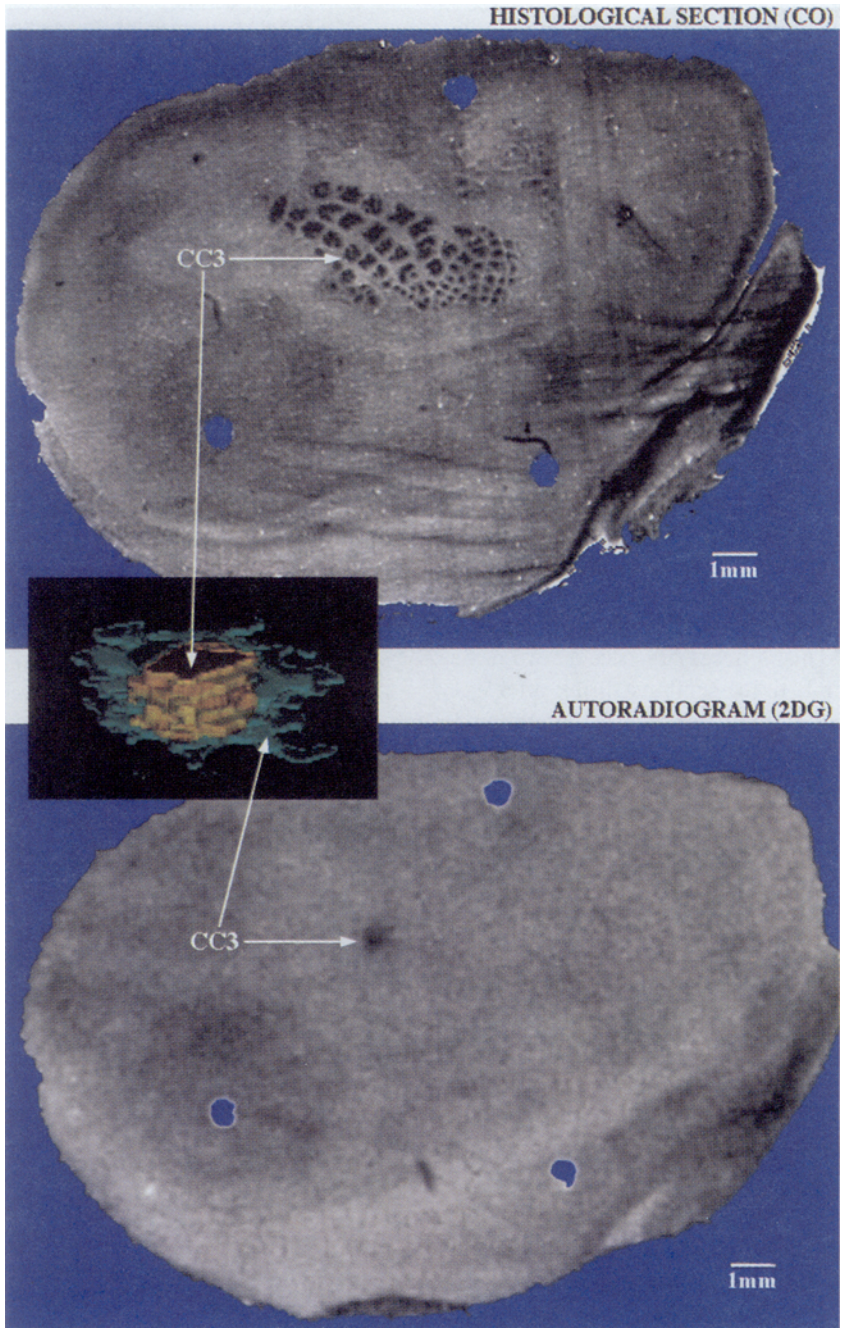

FIGURE 3. (Top) single histological section (anatomical image) of layer IV in the PMBSF of the flattened SI cortex produced with cytochrome oxidase (CO) staining; this cortical image corresponds to the PMBSF ipsilateral to the neonatal lesion; therefore, it is considered the control side. In this section it is possible to visualize the whole barrelfield. The control C3 (CC3) barrel is marked with arrows. (Bottom) corresponding functional (metabolic) representation of the CC3 barrel as labeled by the 2DG autoradiographic technique. Fiduciary marks are visible on both sections. (Inset) 3-D representations of the functional and anatomical columns (10 adjacent sections within layer IV of SI cortex) volume rendered with the ANALYZE software (21). The anatomical column (CO stain) was rendered as an opaque object (red structure), and the associated functional activity (2DG autoradiogram) was rendered as an overlaid transparent object (green structure).

FIGURE 4. (Top) histological (anatomical) representation of the spared C3 (SC3) barrel (together with other barrels) in the PMBSF of the flattened SI cortex contralateral to the lesion (plastic side). This image was produced with CO staining under the condition that all but one whisker and base (SC3) were surgically removed at an early age. (Bottom) Corresponding functional representation of the SC3 barrel produced with the 2DG labeling technique. Fiduciary marks are visible on both sections. (Inset) 3-D reconstructions of 10 adjacent slices within layer IV of SI cortex. The anatomical column was volume rendered as an opaque (violet) structure, and the 2DG metabolic activity associated with this column is shown as an overlaid transparent object (blue structure). Observe that the SC3 barrel underwent an enlargement of its anatomical and functional representations when compared to those representations of the CC3 barrel (Fig. 3). These renderings were done with the ANALYZE software (21). →

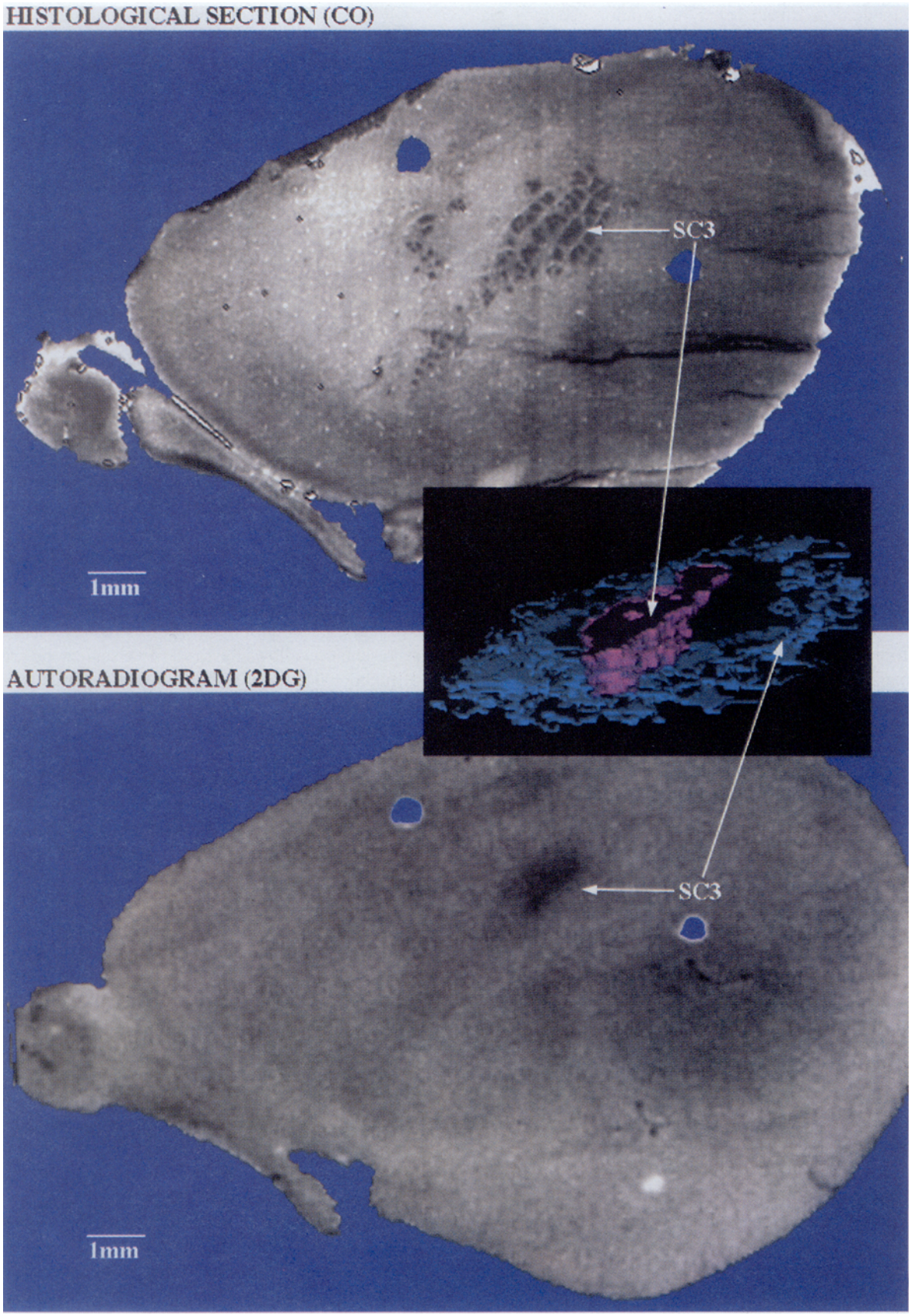
HISTOLOGICAL SECTION (CO)
SC3
1mm
AUTORADIOGRAM (2DG)
SC3
1mm

MSR method produced better registration accuracy than the other methodologies tested. Since the test set used in our experiment was scanned with a resolution of 600 pixels/inch (Agfa flatbed scanner 1200dpi), it indicates that the MSR algorithm yields an accuracy of registration of approximately 40 μm.

EXPERIMENTAL DESIGN

Using the above-mentioned multimodality multidimensional imaging technique, we studied and analyzed normal and altered whisker representations in the rat's cortex and thalamus after selected whisker receptor organ damage. A schematic representation of the sensory pathway between vibrissae located at the rat's face and the corresponding barrels in the thalamus and cortex is shown in Figure 2. A detailed description of our experimental design can be found in Refs. 9 and 16. We will summarize the most important steps in this section. However, those readers seeking additional details should refer to the cited papers.

First, we extracted functional and anatomical information from, respectively, autoradiographic and histological sections. Then we simultaneously registered the sliced data from each modality and the anatomical and functional image volumes. (This is possible because the fiduciary marks impaled on the histological sections are exactly mapped onto the autoradiographic film (refer to Fig. 1); therefore, alignment of the sliced data and registration of the image volumes can be achieved simultaneously.) Finally, we displayed and measured the 3-D functional (metabolic) and anatomical shapes of normal and developmentally altered whisker representations in the first somatosensory area (SI) of the rat cerebral cortex and in the ventrobasal (VB) thalamus. The observed differences between the normal and the developmentally altered whisker representations reflect the degree of cortical and subcortical plasticity (deformation, change) due to neonatal injury of the sensory organs (deafferentation of whiskers vibrissae).

For this study, the metabolic (functional) representations of activated vibrissae follicles within the Posteromedial Barrel Subfield (PMBSF) of SI of the rat neocortex and in the VB thalamus were examined with the quantitative 2DG technique (24). The peripheral stimulation (manually or mechanically controlled brush stroking at 3–5 HZ) was restricted to a single whisker vibrissa (number 3 of row C, C3) to evoke neuronal responses predominantly in one barrel (C3). The 2DG technique was adopted to demonstrate pictorially the global pattern of functional (metabolic) organization of a single cortical and thalamic barrel column. Similarly, the anatomical barrel column representations were studied using the mitochondrial enzyme cytochrome oxidase (CO) (27). Figure 1 illustrates the functional and anatomical representations of a normal (or control) C3 barrel column in the rat's cortex.

RESULTS

We applied the above experimental design to generate multimodality images—2DG and CO—of the control C3 (CC3) barrel column and the spared C3 (SC3) barrel column in the first somatosensory cortex (SI) and in the VB thalamus of the awake, restrained Sprague-Dawley rat. Tangential sections were obtained after three fiduciary marks were placed within the tangential blocks to allow registration of the sections (9).

The upper half of Fig. 3 shows a histological section of layer IV in the PMBSF of SI produced with cytochrome oxidase (CO) staining. This cortical image corresponds to the PMBSF ipsilateral to the neonatal lesion; therefore, it is considered the control side. In this section, it is possible to visualize the whole barrelfield. The CC3 barrel is marked with arrows. The bottom half of Fig. 3 illustrates the functional (metabolic) representation of the CC3 barrel as labeled by the 2DG autoradiographic technique. The inset shows 3-D representations of the functional and anatomic columns (10 adjacent sections within layer IV of SI cortex) rendered with a volume rendering technique (21). In this montage, we rendered the anatomical column (CO stain) as an opaque object (red structure) and the functional activity related to this anatomical column as an overlaid transparent object (green structure). This type of representation allows the reader to visualize the proportion of functional activity associated with a particular anatomical column.

In the upper half of Fig. 4, we have the representation of the SC3 barrel (together with other barrels) in the PMBSF of SI contralateral to the lesion. This anatomical (histological) section was also produced with CO staining. The bottom half of Fig. 4 shows the corresponding functional representation produced with the 2DG labeling technique. Observe that the SC3 barrel underwent an enlargement of its anatomical and functional representations when compared to those representations of the CC3 barrel (Fig. 3). These enlarged (plastic) cortical representations are a consequence of the alterations in the rat's sensory periphery due to a postnatal injury of the contralateral receptor organs, that is, removal of whisker follicles, sparing only the centrally situated C3 whisker and its follicle on one side of the rat's face. The inset shows 3-D reconstructions of 10 adjacent slices within layer IV or SI cortex. The anatomical column was volume rendered as an opaque (violet) structure, and the 2DG metabolic activity associated with this column is shown as an overlaid transparent object (blue structure).

The anatomical and functional images have been registered to each other using the MSR algorithm. The accurate registration procedure allows us to better localize and isolate the site of activation in the low-resolution autoradiograms. Using the ANALYZE software (21), we first

identified and segmented (using thresholding and/or direct editing with a mouse) the individual barrels in the high-resolution histological sections and then superimposed the two images to identify the functional structures in the low-resolution metabolic images. This procedure was applied to both Figs. 3 and 4.

Additionally, to isolate the functional structures of interest from the surrounding background, we first transformed the scanned autoradiograhpic data into concentration units that are proportional to glucose utilization values. Then a global thresholding function was applied to isolate the metabolic signals from the background. In these experiments, a cortical region was considered activated if the local cerebral glucose utilization (LCGU) was 20% higher than the mean background activity. This procedure allows the normalization of data across experiments.

Figure 5 shows 2-D views of the control C3 (top) and the spare C3 (bottom) barreloids at the VB thalamus produced with the 2DG technique. As in the cortex, the SC3 barreloid produced a larger labeling than the CC3 barreloid. Note that the functional barreloids at the thalamus have much smaller dimensions than the corresponding barrels located at layer IV of the SI cortex (also refer to Table 2 for quantitative measurements). Because of their small dimensions, the CO staining technique did not generate good anatomical labeling for CC3 and SC3 barreloids.

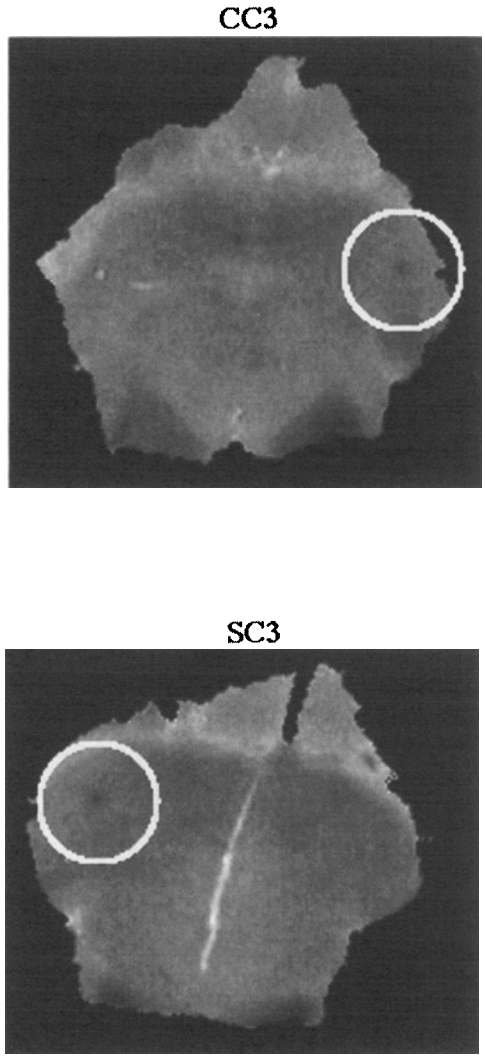

FIGURE 5. (Top) CC3 barreloid at the ventrobasal (VB) thalamus labeled with the 2DG autoradiographic labeling technique. (Bottom) SC3 barreloid at the VB thalamus labeled with the 2DG technique. Note that the SC3 barreloid—which is located contralateral to the neonatal lesion—has produced a larger labeling area than the CC3 barreloid.

DISCUSSION

The results revealed that the cortical plasticity happens in both functional and anatomical levels. On the developmentally altered (injury) side, the neonatal follicle lesions, sparing only the C3 vibrissa, produced an average increase in the volume of cortical tissue driven by the SC3 whisker of more than 150%. The functional cortical plasticity was even larger. The SC3 metabolic column presented an average increase of more than 400% in volume when compared to the CC3 column (refer to Table 2). At the VB thalamus, we found that the plasticity phenomenon is also observed, but to a lesser extent than in the SI cortex. These results, summarized in Table 2, are in agreement with previous observations (9,16).

Several factors could have contributed to the observed anatomical and metabolic plasticity in the SI cortex and VB thalamus, including the following (16): (1) altered development of subcortical, thalamocortical, and cortico-cortical connectivity associated with the vibrissa-SI cortical column pathway; (2) differential development of lamina IV barrels themselves, leading to an underdevelopment of the surrounding denervated barrels and an enlargement of the SC3 anatomical column; (3) reorientation of deafferented barrel neuron dendrites into the territory of the SC3 barrel neurons; and/or (4) unmasking of existing synapses within the territory of some of the denervated barrels associated with the SC3 vibrissa follicle. A more detailed description of these and other factors can be found in Kossut *et al.* (16).

SUMMARY AND CONCLUSIONS

Multimodality multidimensional imaging systems have great potential for enhancing and assisting research in neuroscience. Additionally, the use of image reconstruction and 3-D graphic techniques can greatly improve the visualization of processes and structures being investigated. In this work, we implemented a novel multimodality imaging system that is capable of producing anatomical and functional (metabolic) information of a given structure or pro-

TABLE 2. Two- and three-dimensional measurements of plasticity for five ($N = 5$) subjects (Sprague-Dawley rats).

Brain region	Measurement on 10 Adjacent Slices (25 μm/section)	Control C3	Spared C3 (plastic column)
SI Cortex (layer IV)	Area, 2DG autoradiography	0.65 ± 0.16 mm^2	2.42 ± 0.35 mm^2
	Area, CO staining	0.26 ± 0.08 mm^2	0.50 ± 0.09 mm^2
	Volume, 2DG autoradiography	0.27 ± 0.06 mm^3	0.92 ± 0.17 mm^3
	Volume, CO staining	0.09 ± 0.02 mm^3	0.14 ± 0.03 mm^3
VB thalamus*	Area, 2DG autoradiography	0.09 ± 0.03 mm^2	0.21 ± 0.06 mm^2
	Volume, 2DG autoradiography	0.04 ± 0.01 mm^3	0.09 ± 0.02 mm^3

Average areas (in mm^2) and volumes (in mm^3) of the control C3 (CC3) and spared (C3 (SC3) columns as obtained by 2DG autoradiography and cytochrome oxidase (CO) histochemistry. Quantitative measurements were done with the ANALYZE software (21).
*n = 2 subjects.

cess within the vertebrate's CNS. The functional images are generated from [^{14}C]-2-doexy-D-glucose (2DG) autoradiography, whereas the anatomic images are derived from cytochrome oxidase (CO) histochemistry.

This multimodality imaging technique has been used to study mechanisms underlying information processing in the vertebrate's brain. We have applied this technique to visualize and measure the plasticity (change) observed in the rat's whisker system due to neonatal lesioning of selected peripheral sensory organs (whiskers vibrissae). In these experiments, we rendered and compared individual activated metabolic and anatomical vibrissa columns present in the SI cortex and in the VB thalamus. The findings revealed that in the lesioned side, the C3 metabolic columnar volume increased 450%, on average, when compared to the volume of normal C3 vibrissa columns localized in layer IV of the SI cortex. This plasticity was also observed in the corresponding anatomical representations; however, the order of magnitude of the increase in columnar volume averaged 150% for the side containing the neonatally lesioned sensory organs. A similar but less extensive metabolic plasticity was also observed in the VB thalamus.

Application of this multimodality multidimensional imaging system revealed that we could better understand and study the plasticity phenomena occurring in the rat's whisker system. The metabolic and anatomic structures could be fully visualized, including small changes in the structures' shapes and directionality. Previous 2-D imaging techniques were simply unable to deliver these holistic views.

Another important issue addressed in this work was related to image registration problems. Image registration is an essential preprocessing step executed in most image analysis systems. The presented technique employs fiduciary marks for alignment and is capable of registering images with subpixel accuracy. It uses information from all available fiduciary marks to promote alignment of sections and to avoid propagation of errors across a serial data set.

REFERENCES

1. Apicella, A., J. S. Kippenhan, and J. H. Nagel. Fast multimodality image matching. *SPIE* 1092:252–263, 1989.
2. Arun, K. S., T. S. Huang, and S. D. Blostein. Least-squares fitting of two 3-D sets. *IEEE Trans. Pat. Anal. Mach. Intel.* 9:698–700, 1987.
3. Bajcsy, R., R. Lieberson, and M. Reivich. A computerized system for the elastic matching of deformed radiographic images to idealized atlas images. *J. Comput. Assist. Tomogr.* 7:618–625, 1983.
4. Barrow, H. G., J. M. Tenenbaum, R. C. Bolles, and H. C. Wolf. Parametric correspondence and Chamfer matching: two new techniques for image matching. In: Proceedings of the Fifth International Joint Conference on Artificial Intelligence. Cambridge, MA, 1977, pp. 659–663.
5. Borgefors, G. Hierarchical Chamfer matching: a parametric edge matching algorithm. *IEEE Trans. Pat. Anal. Mach. Intel.* 10:849–865, 1988.
6. Burr, D. J. Elastic matching of line drawings. *IEEE Trans. Pat. Anal. Mach. Intel.* 3:708–713, 1981.
7. Denk, W., K. R. Delaney, A. Gelperin, D. Kleinfeld, B. W. Strowbridge, D. W. Tank, and R. Yuste. Anatomical and functional imaging of neurons using 2-photon laser scanning microscopy. *J. Neurosci. Methods* 54:151–162, 1994.
8. Evans, A. C., S. Marret, L. Collins, and T. M. Peters. Anatomical-functional correlative analysis of the human brain using three dimensional imaging systems. *SPIE* 1092: 264–274, 1989.
9. Goldszal, A. F., O. J. Tretiak, P. J. Hand, S. Bhasin, and D. L. McEachron. Three-dimensional reconstruction of activated columns from 2-[^{14}C]deoxy-D-glucose data. *Neuroimage* 2:9–20, 1995.
10. Gonzalez, R. C., and P. Wintz. *Digital Image Processing* (second edition). Reading, MA: Addison-Wesley, 1987, pp. 425–427.
11. Hand, P. J. Deoxyglucose method. In: *Methods in Contemporary Neuroanatomy: The Tracing of Central Nervous Pathways*, edited by L. Heimes and M. J. Robards. New York: Plenum, 1981, pp. 511–538.
12. Hibbard, L. S., and R. A. Hawkins. Objective image align-

ment for three-dimensional reconstruction of digital autoradiograms. *J. Neurosci. Methods* 26:55–74, 1988.
13. Hibbard, L. S., and R. A. Hawkins. Three-dimensional reconstruction of metabolic data from quantitative autoradiography of rat brain. *Am. J. Physiol.* 247:E412–E419, 1984.
14. Horn, B. K. P. Closed-form solution of absolute orientation using unit quaternions. *J. Opt. Soc. Am. A.* 4:629–642, 1987.
15. Hu, M-K. Visual pattern recognition by moment invariants. *IRE Trans. Inform. Theory* 8:179–187, 1962.
16. Kossut, M., P. J. Hand, J. Greenberg, and C. L. Hand. Single vibrissal cortical column in SI cortex of rat and its alterations in neonatal and adult vibrissa-deafferented animals: A quantitative 2DG study. *J. Neurophysiol.* 60:829–852, 1988.
17. McEachron, D. L., N. T. Adler, and O. J. Tretiak. Two views of functional mapping and autoradiography. *Exp. Biol. Med.* 11:1–46, 1986.
18. Ogawa, S., T. M. Lee, A. S. Nayak, and P. Glynn. Oxygenation-sensitive contrast in magnetic resonance image of rodent brain at high magnetic fields. *Magn. Reson. Med.* 14:68–78, 1990.
19. Pelizzari, C. A., G. T. Y. Chen, D. R. Spelbring, R. R. Weichselbaum, and C-T. Chen. Accurate three-dimensional registration of CT, PET, and/or MR Images of the brain. *J. Comput. Assist. Tomogr.* 13:20–26, 1989.
20. Reisner, A. H., C. A. Bucholtz, G. A. Bell, K. Tsui, D. Rosenfeld, and G. T. Herman. Two- and three-dimensional image reconstructions from stained and autoradiographed Histological sections. *Comput. Appl. Biosci.* 6:253–261, 1990.
21. Robb, R. A., and C. Barillot. Interactive display and analysis of 3-D medical images. *IEEE Trans. Med. Imag.* 8: 217–226, 1989.
22. Schöneman, P. H. A generalized solution of the orthogonal procrustes problem. *Psychometrika* 31:1–10, 1966.
23. Sibson, R. Studies in the robustness of multidimensional scaling: Procrustes statistics. *J. R. Statist. Soc. B* 40:234–238, 1978.
24. Sokoloff, L., M. Reivich, C. Kennedy, M. H. Des Rosiers, C. S. Patlak, K. D. Pettigrew, O. Sakurada, and M. Shinohara. The [^{14}C]deoxyglucose method for the measurement of local glucose utilization: Theory, procedure, and normal values in the conscious and anesthetized albino rat. *J. Neurochem.* 28:897–916, 1977.
25. Toga, A. W., and T. L. Arnicar. Image analysis of brain physiology. *IEEE Comput. Graph. Appl.* 5:20–25, 1985.
26. Tretiak, O. J. Geometrical matching of images: Potential functions and moments. In: Proceedings of the Fifth IEEE International Symposium on Intelligent Control, vol. 1. IEEE Computer Society Press, 1990, pp. 192–199.
27. Wong-Riley, M. Changes in the visual system of monocularly sutured or enucleated cats demonstrated with cytochrome oxidase histochemistry. *Brain Res.* 171:11–28, 1979.
28. Woolsey, T. A. Peripheral alteration and somatosensory development. In: *Development of Sensory Systems in Mammals,* edited by J. R. Coleman. New York: John Wiley and Sons, Inc., 1990, pp. 461–516.